Received: 31 August 2009 ■ *Accepted: 19 October 2009* ■ *Publication: 18 December 2009*

EJMS EUROPEAN JOURNAL OF MASS SPECTROMETRY

Photoelectron spectroscopy and thermochemistry of the peroxyacetate anion

Stephanie M. Villano,[a] Nicole Eyet,[a,b] Scott W. Wren,[a] G. Barney Ellison,[a] Veronica M. Bierbaum[a] and W. Carl Lineberger[a]

[a]JILA, University of Colorado and the National Institute of Standards and Technology and Department of Chemistry and Biochemistry, University of Colorado, Boulder, CO 80309-0440, USA. E-mails: veronica.bierbaum@colorado.edu; wcl@jila.colorado.edu

[b]Current Address: Department of Chemistry, Saint Anselm College, 100 Saint Anselm Dr. #1760 Manchester, NH 03102, USA

The 351.1 nm photoelectron spectrum of the peroxyacetate anion, ($CH_3C(O)OO^-$) was measured. Analysis of the spectrum shows that the observed spectral features arise almost exclusively from transitions between the *trans*-conformer of the anion and the $\tilde{X}^2A''$ and $\tilde{A}^2A'$ states of the corresponding radical. The electron affinity of *trans*-$CH_3C(O)OO$ is 2.381±0.007 eV and the term energy splitting of the $\tilde{A}^2A'$ state is 0.691±0.009 eV, in excellent agreement with two prior values [Zalyubovsky *et al. J. Phys. Chem.* A 107, 7704 (2003); Hu *et al. J. Phys. Chem.* 124, 114305/1 (2006); Hu *et al. J. Phys. Chem.* 110, 2629 (2006)]. The gas-phase acidity of *trans*-peroxyacetic acid was bracketed between the acidity of acetic acid and *tert*-butylthiol at $\Delta_a G_{298}$[*trans*-$CH_3C(O)OOH$] = 1439±14 kJ mol^{-1} and $\Delta_a H_{298}$[*trans*-$CH_3C(O)OOH$] = 1467±14 kJ mol^{-1}. The acidity of *cis*-$CH_3C(O)OOH$ was found by adding a calculated energy correction to the acidity of the *trans*-conformer; $\Delta_a G_{298}$[*cis*-$CH_3C(O)OOH$] = 1461±14 kJ mol^{-1} and $\Delta_a H_{298}$[*cis*-$CH_3C(O)OOH$] = 1490±14 kJ mol^{-1}. The O–H bond dissociation energies for both conformers were determined using a negative ion thermodynamic cycle to be D_0[*trans*-$CH_3C(O)OOH$] = 381±14 kJ mol^{-1} and D_0[*cis*-$CH_3C(O)OOH$] = 403±14 kJ mol^{-1}. The atmospheric implications of these results and relations to the thermochemistry of peroxyacetyl nitrate are discussed briefly.

Keywords: acylperoxy radical, acyl peroxide, peroxyacetyl radical, peroxyacetic acid, photoelectron spectroscopy, FA-SIFT, negative ion cycle, bond dissociation energy, atmospheric chemistry, peroxyacetyl nitrate

Introduction

Organic peroxy radicals (ROO) play an integral role in the chemistry of the troposphere.[1–3] These radicals are formed as a result of OH-initiated oxidation of volatile organic compounds (RH) emitted from biogenic and anthropogenic sources; this process efficiently removes hydrocarbons from the atmosphere and serves as an important sink for the OH radical. Once formed, alkyl radicals (R) rapidly combine with O_2 via a three-body reaction to produce organic peroxy radicals.

$$RH + OH \rightarrow R + H_2O \quad (1)$$

$$R + O_2 + M \rightarrow ROO + M \quad (2)$$

Peroxy radicals react with the NO_x and HO_x radical families. In urban areas, reactions with NO_x species dominate. By oxidizing NO to NO_2, peroxy radicals directly influence tropospheric ozone formation, since the photolysis of NO_2 forms $O(^3P)$, which rapidly reacts with O_2 to form O_3 in the sequence shown below.[4,5]

$$ROO + NO \rightarrow RO + NO_2 \quad (3)$$

$$NO_2 + h\nu \rightarrow NO + O(^3P) \quad (4)$$

$$O(^3P) + O_2 + M \rightarrow O_3 + M \quad (5)$$

In areas of low NO_x, organic peroxy radicals primarily react with other peroxy radicals (mainly HOO), propagating chain reactions that eventually lead to the removal of radicals from the atmosphere.

ISSN: 1469-0667
doi: 10.1255/ejms.1055

Due to their significance in atmospheric chemistry, the structure and thermochemistry of these radicals is of great interest. In particular, the peroxyacetyl radical ($CH_3C(O)OO$) is one of the most abundant peroxy radicals in the atmosphere. In polluted environments, this radical reacts with NO_2 to form peroxyacetyl nitrate (PAN).[6,7]

$$CH_3C(O)OO + NO_2 + M \rightleftharpoons CH_3C(O)OONO_2 + M \qquad (6)$$

PAN is a key component in photochemical smog, it is a respiratory and eye irritant, and can damage vegetation. Due to its stability relative to other peroxynitrates, PAN acts as a temporary reservoir for NO_X species and can undergo long-range transport from areas of high pollution to areas of low pollution, where subsequent thermal decomposition releases the reactive radicals.

The IR spectrum of the peroxyacetyl radical has been reported in a noble gas matrix from the flash thermolysis of PAN.[8] The primary decomposition pathway of PAN was shown to occur by O–N bond fission regenerating the peroxyacetyl radical: $CH_3C(O)OONO_2 + \Delta \rightarrow CH_3C(O)OO + NO_2$. The resulting IR features were attributed to two stable conformers of the peroxyacetyl radical defined by the OCOO dihedral angle.

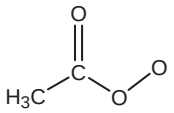

cis

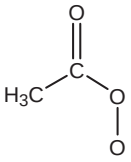

trans

The *trans*-structure is slightly more stable than the *cis*-structure. Therefore, by changing the thermolysis temperature and, hence, the intensity ratio of the two sets of IR bands, spectral features corresponding to both the *cis*- and *trans*-conformers were assigned.

Several spectroscopic and kinetic studies have probed the strong UV $\tilde{B}$–$\tilde{X}$ transition in the peroxyacetyl radical.[9–13] However, due to the repulsive nature of the $\tilde{B}$ state, this transition is broad and featureless, providing few structural details.[2] In contrast, the low-lying $\tilde{A}$–$\tilde{X}$ transition displays rotational and vibrational structure; however, due to its relatively small absorption cross-section, this transition requires use of sensitive spectroscopic techniques. Zalyubovsky *et al*.[14] recorded the gas-phase absorption spectrum of the peroxyacetyl radical produced from photolysis of $(COCl)_2$ in a $CH_3CHO/O_2/N_2$ mixture using cavity ring-down spectroscopy. More recently, Hu *et al*.[15,16] employed near-IR/VUV ion enhancement spectroscopy to record the spectrum of peroxyacetyl radical produced from the thermal decomposition of PAN in a pyrolysis/supersonic pulsed nozzle. The results of these experiments are in excellent agreement with one another. The vibronic features were found to correspond to the *trans*-conformer of the radicals, the $\tilde{A}$–$\tilde{X}$ term energy splitting was determined to be $5582.5 \pm 0.5\,cm^{-1}$ and several $\tilde{A}$ state vibrational modes were identified.

Previously, we have employed negative ion spectroscopy and gas-phase ion–molecule reactivity studies to investigate several peroxy radicals,[17–24] including HOO, CH_3OO, CH_3CH_2OO, $(CH_3)_3COO$, and most recently the peroxyformyl radical, HC(O)OO. Negative ion spectroscopy provides thermodynamic information such as electron affinities (*EA*) and term energies (T_e), allows for the measurement of vibrational frequencies, and gives insight into the molecular structure of radical species as well as the corresponding anion. Gas-phase ion–molecule reactivity studies are used to determine the gas-phase acidity of the corresponding peroxy acid relative to that of a reference acid. These techniques are complementary, since the electron affinity of the radical can be combined with the gas-phase acidity to determine the bond dissociation energy using a negative ion thermochemical cycle.[25–28]

Our recent study of the peroxyformyl radical[24] is particularly relevant to the peroxyacetyl radical and highlights several important differences in the thermochemistry of acylperoxy [RC(O)OO] versus alkylperoxy (ROO) radicals. For example, the *EA* of peroxyformyl radical was found to be 2.493 ± 0.006 eV, which is considerably higher than that of an alkyl peroxy radical, which ranges from 1.0–1.2 eV.[17,18,20] The greater *EA* of the peroxyformyl radical is due to the electron withdrawing effects of the carbonyl group which stabilizes the corresponding anion. The photoelectron spectrum displays extended, partially resolved progressions in the O–O and C–OO stretching modes of the ground state of the *trans*-radical, consistent with the delocalization of the negative charge in the anion across the OCOO backbone. Another important difference in the thermochemistry of the peroxyformyl radical is the significantly larger O–H bond dissociation energy of the corresponding acid; D_0(*cis*-peroxyformic acid) $= 406 \pm 14\,kJ\,mol^{-1}$. Typically O–H bond dissociation energies of peroxy alcohols[17,18,20] range from $350–364\,kJ\,mol^{-1}$. This greater bond strength is attributed to two factors: (1) the strong intramolecular hydrogen bond that is formed between the acylperoxy hydrogen atom and the carbonyl oxygen atom and (2) a reduction in the repulsive interaction between the O–H bonding orbital and lone pair of electrons on the neighboring oxygen atom through electron back-bonding effects.

In this work, we report the negative ion photoelectron spectrum of the peroxyacetate anion [$CH_3C(O)OO^-$]. This technique provides access to the two lowest electronic states of the peroxyacetyl radical through photodetachment of an electron from the corresponding anion. Analysis of the kinetic energy of the detached electron allows for the determination of the *EA* as well as the $\tilde{A}$–$\tilde{X}$ T_e of the peroxyacetyl radical. Additionally, the gas-phase acidity of peroxyacetic acid was measured using an ion–molecule bracketing technique and these measurements are used to determine the O–H bond dissociation energy. Electronic structure calculations provide additional insight into the structural and energetic aspects of the peroxy ion, the radical and the parent acid. The thermochemical values determined here are compared to those of the peroxyformyl radical and the atmospheric implications of these results are briefly discussed in relation to the thermochemistry of peroxyacetyl nitrate (PAN).

Experimental details

Negative ion photoelectron spectroscopy

These studies were carried out with an anion photoelectron spectrometer that has been described in detail elsewhere.[20,29,30] The peroxyacetate anion, $CH_3C(O)OO^-$, was generated in a flowing afterglow source[20] through a series of ion–molecule reactions that occur downstream from a microwave discharge source forming O^- anions.

$$O^- + CH_4 \rightarrow CH_3 + OH^- \quad (7)$$

$$OH^- + H_2O_2 \rightarrow H_2O + HOO^- \quad (8)$$

$$HOO^- + CH_3C(O)OR \rightarrow CH_3C(O)OO^- + ROH \quad (9)$$

The final reaction step utilizes either methyl acetate [$CH_3C(O)OCH_3$], ethyl acetate [$CH_3C(O)OCH_2CH_3$], or 2,2-difluoroethyl acetate [$CH_3C(O)OCH_2CF_2H$]. Due to the large number of collisions in the source region (~0.5 torr, 3–10 ms residence time), ions are prepared with an approximate 298 K rotational and vibrational Maxwell–Boltzmann distribution. Negative ions are gently extracted from the source region and passed though a Wien filter for mass selection. The mass selected ion beam is then crossed with a 351.1 nm (3.531 eV) line from a cw argon-ion laser in an external build-up cavity producing roughly 100 W of circulating power. Photoelectrons that are ejected perpendicular to the ion and photon beams into a small solid angle are analyzed by a hemispherical kinetic energy analyzer coupled to a position-sensitive detector. Spectra are obtained by measuring the photoelectron counts as a function of electron kinetic energy (eKE). The energy scale is converted to electron binding energy (eBE) by subtracting the electron kinetic energy from the photon energy.

The absolute energy scale is calibrated with the well-known electron affinity of the sulfur atom[31] and a linear energy scale compression factor (< 1%), which is derived from the photoelectron spectra of reference ions S^-, I^- and O^- using the *EA*s of the corresponding atoms.[29,31] The electron energy resolution in these experiments is 12–15 meV; however, the electron binding energy corresponding to an isolated transition can easily be determined to an accuracy of ± 5 meV (0.5 kJ mol^{-1}). If that peak is associated with the transition from the ground state of the anion to the ground state of the neutral, the corresponding *EA* can be determined with similar accuracy. Although the presence of unresolved structure reduces the accuracy of the experimental result, Franck–Condon modeling of the full spectrum still allows quantitative assessments of the experimental error in the binding energy measurements.

Angular distribution measurements at a given electron kinetic energy were conducted by changing the angle (θ) between the electric field vector of the laser beam and the photoelectron collection axis. Photoelectrons have an angular distribution according to the expression,[32]

$$\frac{d\sigma}{d\Omega} = \frac{\sigma_{tot}}{4\pi}\left[1 + \beta(eKE)P_2(\cos\theta)\right] \quad (10)$$

where σ_{tot} is the total photodetachment cross section, β is the anisotropy parameter and $P_2(\cos\theta)$ is the second Legendre polynomial. Spectra collected at the magic angle ($\theta = 54.7°$) provide intensities that are free from angular dependence. Spectra collected at $\theta = 0°$ and $\theta = 90°$ allow for determination of the anisotropy parameter.[30]

Flowing afterglow-selected ion flow tube (FA-SIFT) measurements

The gas-phase acidity (Δ_aG_{298}) of peroxyacetic acid was determined using a tandem flowing afterglow-selected ion flow tube instrument, which has been described in detail previously.[33] An ion–molecule bracketing technique[34] was employed. In this method, the peroxyacetate ion is allowed to react with several reference acids (AH) of known acidity. If rapid proton transfer is observed, then the reference compound is a stronger acid than the peroxyacetic acid {$\Delta_aG_{298}[AH] < \Delta_aG_{298}$ [$CH_3C(O)OOH$]}. If proton transfer is not observed then the reference compound is a weaker acid than the peroxyacetic acid {$\Delta_aG_{298}[AH] > \Delta_aG_{298}[CH_3C(O)OOH]$}. The occurrence or non-occurrence of proton transfer with a series of reference acids places an upper and lower bound on the acidity of the peroxyacetic acid. The gas-phase acidity is the free-energy change for heterolytic bond cleavage, $AH \rightarrow A^- + H^+$. Less energy is required to remove a proton from a stronger acid than from a weaker acid; thus, stronger acids have smaller free energy changes than do weaker acids. The enthalpy of deprotonation (Δ_aH_{298}) can be found from Equation (11) where Δ_aS_{298}, the entropy of deprotonation, is estimated from electronic structure calculations.

$$\Delta_aH_{298}[CH_3C(O)OOH] = \Delta_aG_{298}[CH_3C(O)OOH] + T\Delta_aS_{298}[CH_3C(O)OOH] \quad (11)$$

The peroxyacetate anion was formed in a flowing afterglow source using the same synthesis scheme as in the above photodetachment study. Negative ions were extracted from the source region and focused into a quadrupole mass filter, which transmits one specific mass-to-charge ratio ion. The mass selected ion beam was injected into a reaction flow tube where the ions undergo multiple collisions with the He buffer gas (~ 0.5 torr, 10 ms residence time) resulting in an approximate 298 K rotational and vibrational Maxwell–Boltzmann distribution. A measured flow of the neutral reference acid was introduced into the reaction flow tube at various distances through a manifold of inlets. The intensities of the reactant and product ions were measured using a triple quadrupole mass filter coupled to an electron multiplier as a function of reaction time. Neutral reactant flow rates were measured by monitoring the pressure change versus time in a calibrated volume system.

Despite injecting the peroxyacetate anions into the reaction flow tube with minimal energy, fragment ions due to collision-induced dissociation are also present in the reaction flow tube. Since the basicity of some of these fragment ions is greater than that of the peroxyacetate anion, the deprotonated reference acid was observed, even when it is a weaker acid than peroxyacetic acid. Additionally, depletion of the peroxyacetate

anion was also generally observed, since it reacts by neutral oxygen atom transfer. In order to determine whether proton transfer occurs between the peroxyacetate anion and the reference acid, the intensities of all ions were monitored as a function of time and the contribution from the fragment ions to the deprotonated reference acid signal was removed.

Electronic structure calculations

Two theoretical approaches, both provided in the Gaussian 03 suite of programs,[35] were used to evaluate various structural and energetic aspects of the peroxyacetate anion as well as the corresponding radical and protonated species. Optimized geometries, harmonic vibrational frequencies (unscaled), and the rotational constants were calculated using the B3LYP/6-311++G(d,p)[36–38] level of theory. This level of theory was chosen since it has been shown to produce reliable structures for this class of molecules.[24] The G3MP2B3 composite technique[39] was used to investigate various thermodynamic properties of these species. In this technique, geometries and zero point energies are calculated at the B3LYP/6-31G(d) level of theory followed by a series of well-defined *ab initio* single-point energy calculations. This method has been tested on a variety of hydrocarbons, and the average deviation from experiment was reported to be 5 kJ mol^{-1}.[39] Independent evaluation[24] of this method on a series of oxygenated species that are similar in structure to the peroxyacetyl radical suggest a slightly higher deviation of 6 kJ mol^{-1}. Simulated photoelectron spectra were obtained by calculating the Franck–Condon (FC) factors at a vibrational temperature of 298 K using the PESCAL program.[40] These simulations are based on the B3LYP/6-311++G(d,p) optimized geometries and normal modes for the anion and corresponding radical species, while electron binding energies are determined from the G3MP2B3 calculations.

Results and discussion

Photoelectron spectra of the peroxyacetate anion

Figure 1(a) shows the 351.1 nm magic angle photoelectron spectrum of the *m/z* 75 ion produced from the reaction of HOO^- with ethylacetate. The same spectral profile is observed when the *m/z* 75 ion is produced from the reaction of HOO^- with methylacetate and with 2,2-difluoroethylacetate. The anisotropy parameter (β) was measured and is negative across the entire spectrum, consistent with photodetachment from a π-type orbital.[17,18,20] Since this ion is produced from an analogous set of reactions as was the peroxyformate anion in our previous studies,[24] it is likely that the *m/z* 75 ion is the peroxyacetate anion. However, because there is more than one acidic site in peroxyacetic acid, one must consider whether or not deprotonation can also occur at the methyl group to form the hydrogenperoxide ethylenolate anion [$CH_2C(O^-)OOH$] as shown below. Although deprotonation at the OO–H-site is favored thermodynamically (by ~20 kJ mol^{-1}), such lack of selectivity has previously been reported in the deprotonation of acetic acid.[41]

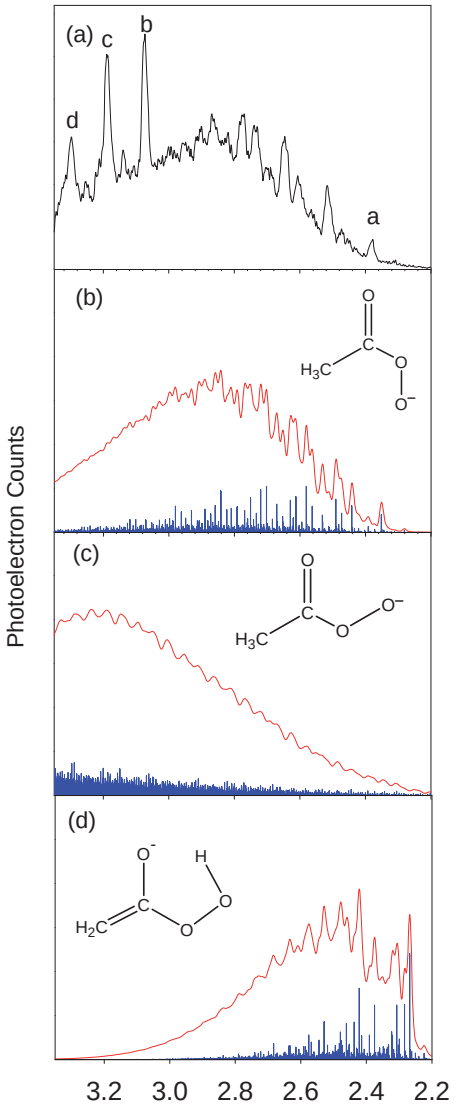

Figure 1. (a) The 351.1 nm magic-angle photoelectron spectrum of the peroxyacetate anion. Franck–Condon simulation for transitions from (b) $\tilde{X}^1A'$ state of the trans-peroxyacetate anion to the $\tilde{X}^2A''$ state of the *trans*-peroxyacetyl radical, (c) $\tilde{X}^1A'$ state of the *cis*-peroxyacetate anion to the $\tilde{X}^2A''$ state of the *cis*-peroxyacetyl radical, and (d) $\tilde{X}^1A'$ state of the hydrogenperoxide ethylenolate anion to the $\tilde{X}^2A''$ state of the hydrogenperoxide ethylenolyl radical. The simulations are based on B3LYP/6-311++G(d,p) optimized geometries and harmonic frequencies; the position of the origin is determined using G3MP2B3 theory. The sticks are the Franck–Condon factors and the solid line is a 13 meV FWHM Gaussian convolution of the spectrum.

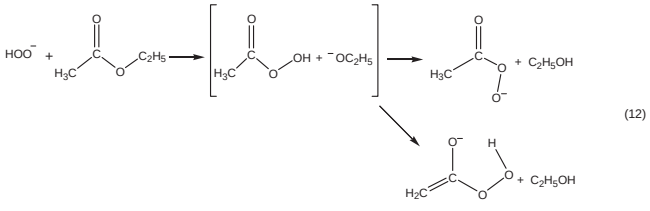

(12)

In order to confirm the identity of the observed spectrum, Franck–Condon simulations were performed. Analogous to the peroxyformate anion,[24] there are two conformations of the peroxyacetate anion (see Table 1). While the *trans*-conformer is predicted to be 24 kJ mol^{-1} more stable than the *cis*-conformer, the two structures are separated by a significant isomerization barrier (70 kJ mol^{-1}), which could potentially trap some of the anion population in the higher energy *cis*-conformation. Thus, spectral simulations were performed for both the *trans*- and *cis*-conformations of the peroxyacetate ion as well as for the hydrogenperoxide ethylenolate ion. These results are summarized in Figure 1(b)–1(d), where the individual vibronic transitions (sticks) are convoluted with a 13 meV FWHM Gaussian function (solid line), which represents the instrument resolution.

The simulated profile for the hydrogenperoxide ethylenolate anion [Figure 1(d)] is inconsistent with the observed spectrum and, therefore, the formation of this isomer is excluded. As mentioned above, the *trans*-conformation is the lowest energy isomer of the peroxyacetate anion and indeed this simulation [Figure 1(b)] is in good agreement with the experiment, reproducing the lower binding energy portion (< 2.8 eV) of the spectrum quite well. The simulation for the *cis*-conformation of the peroxyacetate anion [Figure 1(c)] clearly does not agree with the experimental spectrum. However, since this profile is broad and featureless, it is difficult to exclude all contribution of this conformer from the observed spectrum and, in fact, the *cis*-anion may account for some of the intensity seen at lower binding energies to peak *a* (< 2.3 eV). However, if the *cis*-conformer is present, it is in minor amounts.

The simulation for the *trans*-peroxyacetate anion reproduces the lower binding energy portion of the observed spectrum quite well; however, it does not account for the sharp intense peaks at higher binding energy [shown as peaks *b*, *c*, and *d* in Figure 1(a)]. These peaks are likely due to photodetachment to the $\tilde{X}^2$A′ excited state of the *trans*-peroxyacetyl radical. To confirm this assignment, the Franck–Condon factors for the transition from the $\tilde{A}^1$A′ state of the *trans*-peroxyacetate anion to both the $\tilde{X}^2$A″ and $\tilde{A}^2$A′ states of the corresponding radical were computed and are shown in Figure 2. The sticks correspond to the individual vibronic transitions to the two states of the radical, while the lower trace results from convoluting those individual transitions with a 13 meV FWHM Gaussian function. The calculated electron affinities for both the ground and excited states of the radical have been slightly shifted (< 20 meV) and the intensities normalized to match the experimental spectrum. The excellent quality of the simulation is apparent, especially when one considers the multitude of transitions that contribute to the observed spectrum.

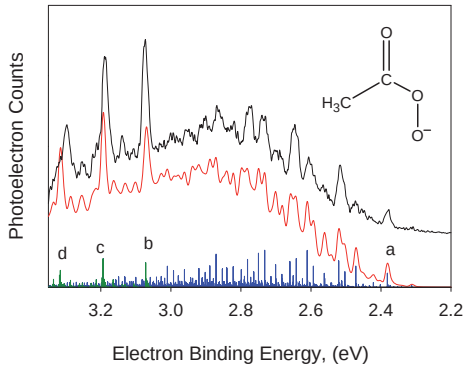

Figure 2. The 351.1 nm magic-angle photoelectron spectrum of the peroxyacetate anion reproduced from Figure 1(a) is shown as the upper trace. Franck–Condon factors are shown for transitions from $\tilde{X}^1$A′ peroxyacetate anion to $\tilde{X}^2$A″ (sticks) and $\tilde{A}^2$A′ (sticks at b, c and d) states of peroxyacetyl radical. The lower trace results from convoluting the stick spectra with a 13 meV FWHM Gaussian function. The energy scale for the simulation is shifted (< 20 meV) and intensities normalized to correspond to the experimental spectrum.

The *EA* of the *trans*-peroxyacetyl radical is determined to be 2.381 ± 0.007 eV, which corresponds to peak *a* in Figure 2. This assignment is in exact agreement with the G3MP2B3 calculated value. The broad features observed at higher binding energies represent excited vibrational levels of the $\tilde{X}^2$A″ state of the *trans*-peroxyacetyl radical. The presence of the methyl group at the carbonyl center leads to more complication and congestion in the ground state vibronic features when compared to the rather simple peroxyformate anion spectrum, which is composed of extended, partially resolved progressions in the O–O and C–OO stretching modes.[24] Five modes are activated upon electron photodetachment of the peroxyacetate anion: the O–O stretch (ν_7), C–OO stretch (ν_8), CCOO backbone deformation (ν_9), OCO bend (ν_{10}) and CCOO breathing motion (ν_{12}). The frequencies of these modes have previously been determined using matrix isolation IR spectroscopy (see Table 2).[8] Similar to the peroxyformyl radical, the frequencies of the O–O and C–OO stretches are within 130 cm^{-1} of each other and, therefore, are only partially resolvable with our instrument resolution. This, combined

Table 1. Relative energies (kJ mol^{-1}) of the *trans*- and *cis*-conformers (going from the *trans*- to the *cis*-structure) calculated at the G3MP2B3 level of theory.

	$\Delta_0 E$	$\Delta_{298} G$	$\Delta_{298} H$	$E^{\ddagger}$ ($E + E_{zpt}$)
$CH_3C(O)OOH$	–21.9	–22.0	–22.9	35.8
$CH_3C(O)OO^-$ ($\tilde{X}^1$A′)	23.8	23.1	24.2	71.2
$CH_3C(O)OO$ ($\tilde{X}^2$A″)	2.9	1.2	3.4	24.5

Table 2. B3LYP/6-311++G(d,p) Harmonic frequencies (cm^{-1}) of *trans*-peroxyacetate anion and *trans*-peroxyacetyl radical. Experimental values are provided in parentheses.

ν	Symmetry	Peroxyacetate anion	Peroxyacetyl radical			
		($\tilde{X}^1$A′)	($\tilde{X}^2$A″)		($\tilde{A}^2$A′)	
1	A′	3116	3164		3164	
2		3033	3061		3043	
3		1676	1898	(1850[a])	1883	
4		1450	1460	(1420[a])	1460	
5		1382	1399	(1367[a])	1391	
6		1325	1184	(1153[a])	1141	(1143.8[b])
7		1010	1121	(1099[a])	1005	(928.4[b]; 929[c]; 916[d])
8		934	978	(972[a])	984	(841.5[b])
9		792	726	(736[a])	751	(759.9[b])
10		562	540	(545[a])	541	(538.1[b]; 539[c])
11		500	505		476	(473.4[b]; 473[c])
12		327	322	(348[a])	272	(269.8[b])
13	A″	3097	3124		3105	
14		1443	1463	(1425[a])	1471	
15		1048	1045	(1029[a])	1062	
16		569	540	(500[a])	556	
17		205	145		180	
18		146	135		141	

[a]Ne or Ar matrix;[53] [b]gas-phase;[16] [c]gas-phase[14]

with the extensive combination band progressions in the CCOO backbone deformation and O–O stretch, adds to the complexity of the spectrum.

The intense narrow peaks appearing at higher electron binding energies are due to photodetachment to the low-lying $\tilde{A}^2$A′ electronic state of the radical. There have been two prior independent measurements of the $\tilde{A}^2A' \leftarrow \tilde{X}^2A''$ transition in the *trans*-$CH_3C(O)OO$ radical;[14–16] the splitting between the two states has been accurately determined to be 0.69214 ± 0.00006 eV. This energy splitting, relative to peak *a*, corresponds to peak *b*, which is assigned as the $\tilde{A}^2$A′ electronic band origin. Thus, the $\tilde{A}$–$\tilde{X}$ T_e is determined to be 0.691 ± 0.009 eV, which is in good agreement with the two previous measurements[14–16] and with the G3MP2B3 calculated value of 0.70 eV. The peaks at higher binding energies, peaks *c* and *d*, are the fundamental and first overtone of the O–O stretch (ν_7); the frequency of this mode is determined to be 916 ± 45 cm^{-1}.

Gas-phase acidity measurements

Since the peroxyacetic acid reagent is not available in pure form, the gas-phase acidity of this compound was determined using an ion–molecule bracketing technique rather than a proton transfer equilibrium technique. This bracketing method allows for the determination of the gas-phase acidity of a compound through the examination of the occurrence, or non-occurrence, of proton transfer with several acids. In this manner, the acidity of the compound can be placed between two known acidity values with an error bar that spans the difference in values.

The gas-phase acidity of peroxyacetic acid was bracketed against five reference acids: formic acid (1417 ± 2 kJ mol^{-1}), acetic acid (1428 ± 2 kJ mol^{-1}), hydrogen sulfide (1443.0 ± 0.1 kJ mol^{-1}), *tert*-butylthiol (1451 ± 2 kJ mol^{-1}) and ethanethiol (1461 ± 2 kJ mol^{-1}).[42,43] Proton transfer was not observed in the reactions of peroxyacetate anion with *tert*-butylthiol and ethanethiol; instead, these reactions proceed via neutral oxygen–atom loss to form the acetate anion. Proton transfer was observed in the reactions of formic acid and acetic acid. For the latter reaction, the occurrence of proton transfer was confirmed by evaluating the reaction with acetic acid-d_3, $CD_3C(O)OH$, where the formation of *m/z* 62, instead of *m/z* 59, is consistent with proton transfer. The reaction with hydrogen sulfide produces small amounts of the proton transfer product in addition to the oxygen–atom transfer product, suggesting that this reaction is slightly endothermic. Thus, the acidity of peroxyacetic acid is determined to be between that of acetic acid and *tert*-butylthiol at $\Delta_a G_{298} = 1439 \pm 14$ kJ mol^{-1}.

It has previously been shown using microwave spectroscopy that the lowest energy structure of peroxyacetic acid is

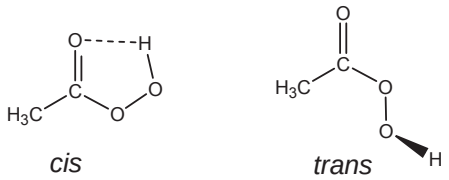

a *cis*-planar structure, where a strong intramolecular hydrogen bond exists between the peroxy hydrogen atom and the carbonyl oxygen atom.[44] Rotation about the OCOO dihedral angle by 180° gives a higher energy *trans*-conformation, where the peroxy hydrogen atom points out of the plane of symmetry.

Using G3MP2B3 theory, we have calculated the relative energetics of these two conformers; these results are summarized in Table 1. At this level of theory, the *trans*-conformer is predicted to be approximately 23 kJ mol^{-1} higher in energy than the *cis*-conformer; a barrier of about 36 kJ mol^{-1} (*trans* to *cis*) separates the two structures. Although this isomerization barrier height is less than a typical ion–dipole complexation energy (60–80 kJ mol^{-1}),[45] proton transfer is generally barrierless and, therefore, proton transfer rather than isomerization is expected to occur. Since the anion exists in the *trans*-conformation, protonation initially forms the higher energy *trans*-conformation of the acid. If proton transfer is sufficiently exothermic, then the acid can transverse the isomerization barrier to form the lower energy *cis*-conformation. However, if proton transfer is not sufficiently exothermic, then the acid will be trapped in the higher energy *trans*-configuration. Analogous conformation differences have been discussed in relation to the acidity measurements of peroxyformic acid.[24]

In these bracketing experiments, the difference in the acidities of the upper and lower bound reference acids is smaller than the isomerization barrier. As a result, the above acidity measurement of $\Delta_a G_{298} = 1439 \pm 14$ kJ mol^{-1} corresponds to the higher energy *trans*-form of the peroxyacetic acid. The gas-phase acidity of the lower energy *cis*-conformer can be determined by calculating the relative stability of the two isomers (Table 1). In this case, computations are expected to accurately predict this energy difference since the systematic errors from the *ab initio* method are similar for both conformers and, therefore, cancel. The gas-phase acidity of *cis*-peroxyacetic acid is determined to be 1461 ± 14 kJ mol^{-1}. Combining these results with the calculated entropies of deprotonation ($\Delta_a S_{298}$) allows for the determination of the enthalpies of deprotonation [Equation (11)]: $\Delta_a H_{298}$(*cis*-$CH_3C(O)OOH$) = 1490 ± 14 kJ mol^{-1}; $\Delta_a H_{298}$(*trans*-$CH_3C(O)OOH$) = 1467 ± 14 kJ mol^{-1}. In both cases, deprotonation leads to the lower energy *trans*-conformation of the anion. With appropriate heat capacity corrections (determined by electronic structure calculations), these acidities can be converted to 0 K values: $\Delta_a H_0$(*cis*-$CH_3C(O)OOH$) = 1485 ± 14 kJ mol^{-1}; $\Delta_a H_0$(*trans*-$CH_3C(O)OOH$) = 1464 ± 14 kJ mol^{-1}.

$$\Delta_a H_0[CH_3C(O)OOH] = \Delta_a H_{298}[CH_3C(O)OOH] - \int_0^{298} \left\{C_p[CH_3C(O)OO^-] + C_p[H^+] - C_p[CH_3C(O)OOH]\right\} dT \quad (13)$$

Thermochemistry

The O–H bond dissociation energy of peroxyacetic acid can be determined from the data measured here using a negative ion/*EA* thermochemical cycle [Equation (14)].[25–28]

$$D_0[CH_3C(O)OO{-}H] = \Delta_a H_0[CH_3C(O)OOH] + EA[CH_3C(O)OO] - IE(H) \quad (14)$$

Here, $\Delta_a H_0(CH_3C(O)OOH)$ is the OH deprotonation enthalpy of peroxyacetic acid at 0 K, $EA(CH_3C(O)OO)$ is the electron affinity of the peroxyacetyl radical and IE(H) is the ionization energy of the hydrogen atom (13.59844 eV). Application of Equation (14) yields D_0[*trans*-$CH_3C(O)OO{-}H$] to be 381 ± 14 kJ mol^{-1} and D_0[*cis*-$CH_3C(O)OO{-}H$] to be 403 ± 14 kJ mol^{-1}. In both cases, O–H bond cleavage leads to the lower energy *trans*-conformation of the radical as shown in Figure 3(a).The uncertainty in the bond energy measurements primarily reflects the error in the gas-phase acidity measurements. A small thermochemical correction is needed to bring the bond dissociation energy of peroxyacetic acid from 0 K to 298 K, shown in Equation (15).

$$D_{298}[CH_3C(O)OO{-}H] = D_0[CH_3C(O)OO{-}H] + \int_0^{298} [C_p(CH_3C(O)OO) + C_p(H) - C_p(CH_3C(O)OOH)]\, dT \quad (15)$$

Application of Equation (15) yields D_{298}[*trans*-$CH_3C(O)OO{-}H$] to be 385 ± 14 kJ mol^{-1} and D_{298}[*cis*-$CH_3C(O)OO{-}H$] to be 408 ± 14 kJ mol^{-1}.

The heat of formation of peroxyacetic acid has not been experimentally determined. Using G3MP2B3 electronic structure calculations, we have calculated the heat of formation of peroxyacetic acid from an isodesmic reaction:

$$CH_3C(O)OOH + H_2O \rightarrow CH_3C(O)OH + H_2O_2 \quad (16)$$

The heat of formation of the peroxy acid is determined from the calculated heat of reaction and the known heats of formation of the other three compounds.[46] Since the bonding environments in the reactants and products are similar, the systematic errors from the *ab initio* method cancel and, therefore, this approach is expected to produce reasonably accurate heats of formation for closed shell species. Using this method, the heat of formation at 298 K of the *cis*-peroxyacetic acid was found to be –348 ± 4 kJ mol^{-1}, in good agreement with the calculations of Bozzelli *et al.*[47] and Benassi *et al.*[48] The error bar reflects the uncertainty in the heats of formation of $CH_3C(O)OH$, H_2O_2 and H_2O, as well as an estimated uncertainty of 2 kJ mol^{-1} in the calculated heat of reaction.

The heat of formation of the *trans*-peroxyacetyl radical, $\Delta_f H_{298}[CH_3C(O)OO)]$ can be determined from the calculated heats of formation of the peroxyacetic acid [$\Delta_f H_{298}[CH_3C(O)OOH)]$] and the above O–H bond energy measurement [$D_{298}[CH_3C(O)OO{-}H]$ using Equation (17), where the heat of formation of hydrogen atom[49] [$\Delta_f H_{298}$(H)] is 217.999 ± 0.004 kJ mol^{-1}.

$$\Delta_f H_{298}[CH_3C(O)OO] = D_{298}[CH_3C(O)OO{-}H] + \Delta_f H_{298}[CH_3C(O)OOH] - \Delta_f H_{298}(H) \quad (17)$$

Table 3. Thermochemical parameters.[a]

Peroxyacetyl radical and peroxyacetic acid	
EA(*trans*-$CH_3C(O)OO$)	2.381 ± 0.007 eV
T_e $\tilde{A}$–$\tilde{X}$ (*trans*-$CH_3C(O)OO$)[b]	0.69214 ± 0.00006 eV
$\Delta_a G_{298}$(*trans*-$CH_3C(O)OO$–H)[c]	1439 ± 14 kJ mol^{-1}
$\Delta_a G_{298}$(*cis*-$CH_3C(O)OO$–H)[d]	1461 ± 14 kJ mol^{-1}
$\Delta_a H_{298}$(*trans*-$CH_3C(O)OO$–H)[e]	1467 ± 14 kJ mol^{-1}
$\Delta_a H_{298}$(*cis*-$CH_3C(O)OO$–H)[e]	1490 ± 14 kJ mol^{-1}
D_0(*trans*-$CH_3C(O)OO$–H)[f]	381 ± 14 kJ mol^{-1}
D_0(*cis*-$CH_3C(O)OO$–H)[f]	403 ± 14 kJ mol^{-1}
Peroxyformyl radical and peroxyformic acid[g]	
EA(*trans*-$HC(O)OO$)	2.493 ± 0.006 eV
T_e $\tilde{A}$–$\tilde{X}$ (*trans*-$HC(O)OO$)	$0.783\ ^{+0.060}_{-0.020}$ eV
$\Delta_a G_{298}$(*trans*-$HC(O)OO$–H)[c]	1439 ± 14 kJ mol^{-1}
$\Delta_a G_{298}$(*cis*-$HC(O)OO$–H)[d]	1451 ± 14 kJ mol^{-1}
$\Delta_a H_{298}$(*trans*-$HC(O)OO$–H)[e]	1469 ± 14 kJ mol^{-1}
$\Delta_a H_{298}$(*cis*-$HC(O)OO$–H)[e]	1483 ± 14 kJ mol^{-1}
D_0(*trans*-$HC(O)OO$–H)[f]	393 ± 14 kJ mol^{-1}
D_0(*cis*-$HC(O)OO$–H)[f]	406 ± 14 kJ mol^{-1}

[a]All energy changes correspond to formation of the *trans*-conformation of the anion or radical, which are the most stable forms; [b]Zalyubovsky *et al*.;[14] T_e = 0.691 ± 0.009 eV, this work; [c]Bracketed between the acidity of acetic acid and *tert*-butylthiol; [d]Determined from the acidity of *trans*-peroxy acid and the calculated energy difference between *cis*- and *trans*-conformers; [e]Calculated from the corresponding $\Delta_a G_{298}$ and $\Delta_a S_{298}$; [f]Calculated using the EA,$\Delta_a H_0$, IE(H) [g]Villano *et al*.[24]

Application of Equation (17) yields $\Delta_f H_{298}$[*trans*-$CH_3C(O)OO$] = –158 ± 14 kJ mol^{-1}.

Table 3 compares the thermochemical parameters for the peroxyacetyl radical and peroxyacetic acid determined in this study to our recently published values for the peroxyformyl radical and peroxyformic acid.[24] The thermochemical parameters for these two peracids are similar to one another. While the *EA* of the peroxyacetyl radical is slightly lower than that of the peroxyformyl radical, the gas-phase acidities of peroxyacetic acid and peroxyformic acid are the same within our experimental error. Moreover, the O–H bond dissociation energies of these peracids are similar, but substantially larger than those for peroxy alcohols,[17,18,20] which range from 350–364 kJ mol^{-1}. The greater bond strength can be understood in terms of the strong intramolecular hydrogen bond in the peracid, as well reduced lone pair-bonding pair repulsion through electron back-bonding effects.[24] An extensive set of bond dissociation energies and heats of formation at 0 and 298 K for the *cis*- and *trans*-conformers of both peroxyacetic acid and peroxyformic acid are presented in Figure 3.

Atmospheric and environmental implications

The unexpected bond strengths of organic peracids, roughly 400 kJ mol^{-1} (see Figure 3), sheds light on several problems in the atmospheric and environmental processing of aldehydes.

It is well known that samples of aldehydes that have been exposed to air are rapidly contaminated by carboxylic acids: RCHO + "air" → RC(O)OH. This is known to be a radical chain process in solution that is initiated by a radical abstraction from the aldehyde. A radical chain then ensues.

$$RCHO + \text{radical} \rightarrow RC(O) \qquad [18(a)]$$

$$RC(O) + O_2 \rightarrow RC(O)OO \qquad [18(b)]$$

$$RC(O)OO + RCHO \rightarrow RC(O)OOH + RC(O) \qquad [18(c)]$$

Over time, the air oxidizes the aldehyde to a peracid. The peracid subsequently destroys the aldehyde via a Baeyer–Villiger oxidation:

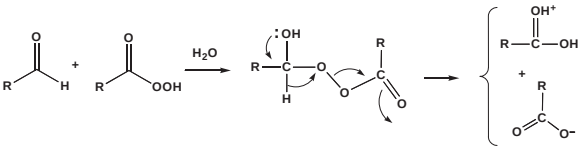

(19)

The bond strength[26] of an aldehyde, D_{298}[RC(O)–H], is about 370 kJ mol^{-1} while that of a peroxyalcohol, D_{298}(ROO–H), is approximately 350 kJ mol^{-1}. Consequently, step [18(c)] is roughly 20 kJ mol^{-1} endothermic. However, the experimental bond energies in Figure 3 change the thermochemistry of [18(c)]. Our measured value for D_{298}[*cis*-$CH_3C(O)OO$–H → *trans*-$CH_3C(O)OO$ + H] of 408 ± 14 kJ mol^{-1} now makes the H atom abstraction exothermic by about 38 kJ mol^{-1}.

In the atmosphere, a common fate of aldehydes is oxidation by OH radical to generate acyl radicals. These acyl radicals rapidly combine with oxygen to produce peroxyacyl radicals.[50,51]

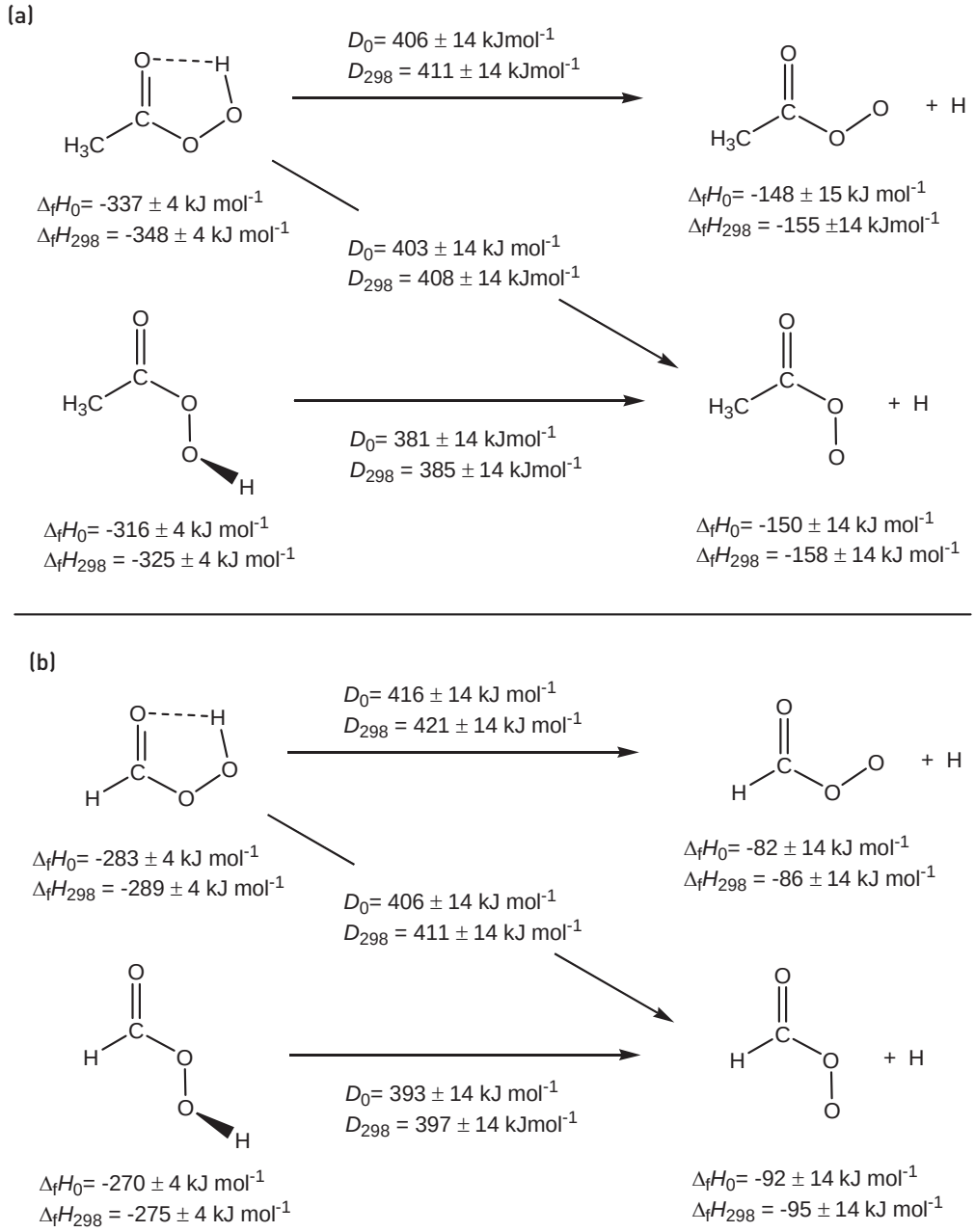

Figure 3. (a) Thermochemistry of peroxyacetic acid at 0 and 298 K. The heat of formation of peroxyacetic acid is calculated at the G3MP2B3 level of theory [Equation (16)]. The bond dissociation energies are experimentally determined here [Equation (14); a small energy correction is applied to the bond dissociation energy for *cis*-$CH_3C(O)OOH \rightarrow$ *trans*-$CH_3C(O)OO + H$ and for *cis*-$CH_3C(O)OOH \rightarrow$ *cis*-$CH_3C(O)OO + H$ (see text). The heat of formation of the peroxyacetyl radical is determined from the heat of formation of peroxyacetic acid and the corresponding bond dissociation energy [Equation (17)]. (b) Thermochemistry of peroxyformic acid (Villano *et al.*[24]) at 0 and 298 K.

$$RCHO + OH \rightarrow H_2O + RC(O)\ [+O_2] \rightarrow RC(O)OO \qquad (20)$$

In the case of formaldehyde, the resulting peroxyformyl radical is chemically-activated by 138 ± 14 kJ mol^{-1}; this exothermicity is determined as the difference in the heats of formation of the *trans*-peroxyformyl radical and the formyl radical.

$$HC(O) + O_2 \rightarrow HC(O)OO \qquad (21)$$

Therefore, the peroxyformyl radical is internally excited by approximately 11,500 cm^{-1} and can rearrange to CO + HOO. The $\Delta_{rxn}H_{298}[HC(O)OO \rightarrow CO + HOO]$ is computed[46] to be −2 ± 14 kJ mol^{-1}.

Oxidation of acetaldehyde by OH / O_2 yields peroxyacetyl radicals that are chemically-activated as well. For *trans*-$CH_3C(O)OO$, the internal excitation can be calculated[26]

Thermochemisry Chart: Peroxyacetyl Nitrate (PAN)

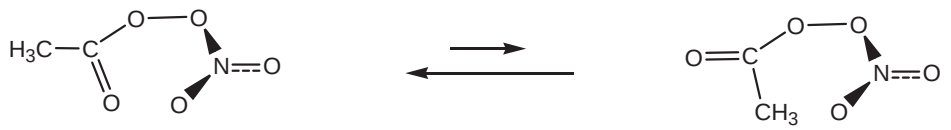

trans, trans, gauche-PAN

B3LYP/6-311G(d,p) calculated
$\Delta E(t,t,g \rightarrow t,c,g) = 13.2$ kJ mol^{-1}
von Ahsen *et al.*[8]

trans, cis, gauche-PAN

$\Delta_f H_0(CH_3C(O)OONO_2) = -229 \pm 15$ kJ mol^{-1}
$\Delta_f H_{298}(CH_3C(O)OONO_2) = -243 \pm 15$ kJ mol^{-1}
Derived from this work.

Figure 4. Thermochemistry of peroxyacetyl nitrate.

from $\Delta_f H_{298}(CH_3CO)$ and $\Delta_f H_{298}$[*trans*-$CH_3C(O)OO$] in Figure 3.

$$CH_3C(O) + O_2 \rightarrow \textit{trans}\text{-}CH_3C(O)OO \qquad (22)$$

Oxidation of CH_3CHO by OH/O_2 produces *trans*-$CH_3C(O)OO$ that is internally excited by 148 ± 14 kJ mol^{-1} or 12,380 cm^{-1}. Some of the chemically activated peroxyacetyl radicals decompose[52] to ketene and the peroxyl radical. The $\Delta_{rxn}H_{298}$[$CH_3C(O)OO \rightarrow CH_2CO + HOO$] is evaluated as 124 ± 15 kJ mol^{-1}. Most of the peroxyacetyl radicals do not rearrange but are stabilized by atmospheric collisions.

As mentioned in the introduction, $CH_3C(O)OO$ radicals react with NO_2 in the atmosphere to generate PAN ($CH_3C(O)OONO_2$). This process has been extensively studied experimentally[8,52] and computationally.[8,53] The structure of PAN has been the subject of electronic structure calculations [CBS-Q and B3LYP/6-311G(d,p) methods] and it was discovered that there are two important conformers. These conformers are shown in Figure 4; the *trans, trans, gauche* conformer is slightly more stable than the *trans, cis, gauche* species.

The kinetics for the formation of PAN have previously been studied.[54]

$$CH_3C(O)OO + NO_2 \rightleftharpoons EQN\ CH_3C(O)OONO_2 \qquad (23)$$

The rate constants, k_{23} and k_{-23}, were measured to find $K_{equi}(23)$. From the temperature dependence of the equilibrium constant, the enthalpy change is commonly determined by the van't Hoff Equation. However because of the narrow temperature range, $\Delta_{rxn}H_{298}(23)$, was determined by the third law method.[25] This approach uses a single value of the K_{equi} and relies on equilibrium statistical mechanics to calculate the entropy change. Since the structural parameters of the reactants and products (vibrational frequencies and moments of inertia) can be estimated, their absolute entropy and the entropy of the reaction $\Delta_{rxn}S_{298}$ were calculated. The enthalpy of reaction[54] was found to be $\Delta_{rxn}H_{298}(23) = 118.8 \pm 4.0$ kJ mol^{-1} and $\Delta_{rxn}H_0(23) = 115.1 \pm 4.0$ kJ mol^{-1}.

We can use the thermochemistry of $CH_3C(O)OO$ in Figure 3, together with known[46] properties of NO_2, NO_3, and $CH_3C(O)O$, to deduce the energetics of PAN.

$$\Delta_f H_{298}[CH_3C(O)OO\text{–}NO_2] = \Delta_{rxn}H_{298}(23) + \Delta_f H_{298}[\textit{trans}\text{-}CH_3C(O)OO] + \Delta_f H_{298}(NO_2) \qquad (24)$$

Evaluation of Equation (24) yields $\Delta_f H_{298}$[$CH_3C(O)OO$–NO_2] = –243 ± 15 kJ mol^{-1}. The heat of formation of PAN can be used to find the threshold for the formation of the oxyacetyl and nitrate radicals.

$$CH_3C(O)OONO_2 \rightarrow CH_3C(O)O + NO_3 \qquad (25)$$

The $\Delta_{rxn}H_{298}(25)$ is evaluated as $\leqslant 142 \pm 15$ kJ mol^{-1} or 11,850 cm^{-1}. This would correspond to a photodissociation threshold of $\lambda_{thresh} = 844$ nm.

It is instructive to compare these thermochemical results for PAN with those resulting from electronic structure calculations. Two important papers[8,53] use the CBS-Q and the B3LYP/6-311G(d,p) methods to calculate the heats of formation of PAN as well as for the *trans*-$CH_3C(O)OO$ and $CH_3C(O)O$ radicals. These papers also calculate the reaction enthalpies for PAN. Table 4 presents a comparison of the experimental values with these computational values. It is important to recognize that this experimental study and the CBS-Q calculation of $\Delta_{rxn}H_{298}$[*trans*-$CH_3C(O)OONO_2 \rightarrow$ *trans*-$CH_3C(O)OO + NO_2$] are anchored to the experimental value for this dissociation energy.[54] The experimental uncertainties are largely determined by the bracketing technique that was required to measure the $\Delta_a H_{298}$[$CH_3C(O)OO$–H] values. Nevertheless the experimental findings in Table 4 suggest that the PAN decomposition route generating NO_2 is about 23 kJ mol^{-1} lower than the pathway that generates NO_3. We should note that the calculation of the nitrate path, $\Delta_{rxn}H_{298}$[*trans*-$CH_3C(O)OONO_2 \rightarrow CH_3C(O)O + NO_3$] will be very difficult because NO_3 ($^2E_1''$) is subject to Jahn–Teller distortion. Likewise the oxylacetyl radical, $CH_3C(O)O$, is metastable. All experimental evidence suggests that $CH_3C(O)O$ instantly decomposes to $CO_2 + CH_3$. Indeed, this is the source of CO_2 in the matrix studies reported by von Ahsen *et al.*[8]

Table 4. Energetics for PAN decomposition (kJ mol^{-1}).

Process	Values deduced from this work	CBS-Q calc.[a]	B3LYP/6-311G(d,p)[b]
$\Delta_f H_{298}(CH_3C(O)OONO_2)$	−243 ± 15[c]	−240 ± 7	
$\Delta_f H_{298}$(*trans* $CH_3C(O)OO$)	−158±14[d]	−154 ± 6	
$\Delta_f H_{298}(CH_3CO_2)$	⩽ −175 ± 4[e]	−193 ± 6	
$\Delta_{rxn} H_{298}(CH_3C(O)OONO_2 \rightarrow$ *trans*-$CH_3C(O)OO + NO_2)$	118.8 ± 4.0[f]	119 ± 4	92.0
$\Delta_{rxn} H_{298}(CH_3C(O)OONO_2 \rightarrow$ $CH_3CO_2 + NO_3)$	⩽ 142 ± 15[e]	121 ± 8	94.3
$\Delta_{rxn} H_{298}(CH_3C(O)OONO_2 \rightarrow$ $CH_3 + CO_2 + NO_3)$	70 ± 15[e]		50.0
$\Delta_{rxn} H_{298}(CH_3CO_2 \rightarrow$ $CH_3 + CO_2)$	⩾ −72 ± 4[e]		−42.0
$\Delta_{rxn} H_{298}$(*trans*-$CH_3C(O)OO + NO_2 \rightarrow$ $CH_3CO_2 + NO_3)$	⩽ 23 ± 15[e]	2 ± 7	
$\Delta_{rxn} H_{298}$(*trans*-$CH_3C(O)OO \rightarrow$ $CH_2CO + HOO)$	124 ± 15[e]	122.4	

[a]Miller *et al.*;[53] von Ahsen *et al.*;[8] [c]From Equation (24); [d]From Equation (17); [e]Heats of formation of radicals and compounds not determined in this work are given in footnote 46; [f]Bridier *et al.*[54]

Conclusions

The 351.1 nm photoelectron spectrum of the peroxyacetate anion was measured and is in good agreement with the calculated Franck–Condon factors for the $\tilde{X}^1A'$ state of the *trans*-conformer of the anion to the $\tilde{X}^2A''$ and $\tilde{A}^2A'$ states of the corresponding radical. The *EA* of the *trans*-$CH_3C(O)OO$ is 2.381 ± 0.007 eV and the T_e of the $\tilde{A}^2A'$ states is 0.691 ± 0.009 eV, which is in excellent agreement with two prior values.[14–16] The gas-phase acidity of *trans*-peroxyacetic acid was bracketed between the acidity of acetic acid and *tert*-butylthiol at $\Delta_a G_{298}$[*trans*-$CH_3C(O)OOH$] = 1439 ± 14 kJ mol^{-1} and $\Delta_a H_{298}$[*trans*-$CH_3C(O)OOH$] = 1467 ± 14 kJ mol^{-1}. The acidity of *cis*-$CH_3C(O)OOH$ acid was found by adding a calculated energy correction to the acidity of the *trans*-conformer; $\Delta_a G_{298}$[*cis*-$CH_3C(O)OOH$] = 1461 ± 14 kJ mol^{-1} and $\Delta_a H_{298}$[*cis*-$CH_3C(O)OOH$] = 1490 ± 14 kJ mol^{-1}. The O–H bond dissociation energies for both conformers were determined using a negative ion thermodynamic cycle to be D_0[*trans*- $CH_3C(O)OOH$] = 381 ± 14 kJmol^{-1} and D_0[*cis*-$CH_3C(O)OOH$] = 403 ± 14 kJ mol^{-1}.

Acknowledgments

We are grateful to Professor John F. Stanton, Professor Kent M. Ervin and Professor Charles H. DePuy for helpful discussions and suggestions. Additionally, we acknowledge Ms Kristen M. Vogelhuber for assisting in the photoelectron spectroscopy experiments. This work is supported by the AFOSR (FA9550-09-1-0046). WCL acknowledges support from the NSF (CHE0809391 and PHY0551010), VMB acknowledges support from the NSF (CHE-0647088) and GBE acknowledges support from the DOE (DE-FG02-93ER14364) and the NSF (CHE-0848606). The computational results are based upon work supported by the National Science Foundation under the following NSF programs: Partnerships for Advanced Computational Infrastructure, Distributed Terascale Facility (DTF) and Terascale Extensions: Enhancements to the Extensible Terascale Facility.

References

1. G. Le Bras, "Chemical processes in atmospheric oxidation: laboratory studies of chemistry related to tropospheric ozone", in *Transport and Chemical Transformation Of Pollutants in the Troposphere*, Vol. 3, Ed by G. Le Bras. Springer, Berlin, Germany, p. 13 (1997).

2. P.D. Lightfoot, R.A. Cox, J.N. Crowley, M. Destriau, G.D. Hayman, M.E. Jenkin, G.K. Moortgat and F. Zabel, "Organic peroxy-radicals—kinetics, spectroscopy and tropospheric chemistry," *Atmos. Environ. Part A* **26,** 1805–1961 (1992).

3. S. Madronich, J. Greenberg, S. Paulson, J.J. Orlando, and G.S. Tyndall, "Organic compounds", in *Atmospheric Chemistry and Global Change*, Ed by G.P. Brasseur, J.J. Orlando and G.S. Tyndall. Oxford University Press, Oxford, UK, p. 325–345 (1999).

4. B.J. Finlayson-Pitts and J.N. Pitts, "Tropospheric air pollution: ozone, airborne toxics, polycyclic aromatic

hydrocarbons, and particles", *Science* **276,** 1045–1052 (1997). doi: 10.1126/science.276.5315.1045

5. F. Kirchner and W.R. Stockwell, "Effect of peroxy radical reactions on the predicted concentrations of ozone, nitrogenous compounds, and radicals", *J. Geophys. Res.-Atmos.* **101,** 21007–21022 (1996).

6. J.M. Roberts, "The atmospheric chemistry of organic nitrates," *Atmos. Environ., Part A* **24,** 243–287 (1990).

7. H.B. Singh, D. Herlth, D. Ohara, K. Zahnle, J.D. Bradshaw, S.T. Sandholm, R. Talbot, P.J. Crutzen and M. Kanakidou, "Relationship of peroxyacetyl nitrate to active and total odd nitrogen at northern high-latitudes—influence of reservoir species on NO_x and O_3", *J. Geophys. Res.-Atmos.* **97,** 16523–16530 (1992).

8. S. von Ahsen, H. Willner and J.S. Francisco, "Thermal decomposition of peroxy acetyl nitrate $CH_3C(O)OONO_2$", *J. Chem. Phys.* **121,** 2048–2057 (2004). doi: 10.1063/1.1767813

9. M.A. Crawford, T.J. Wallington, J.J. Szente, M.M. Maricq and J.S. Francisco, "Kinetics and mechanism of the acetylperoxy + HO_2 reaction", *J. Phys. Chem. A* **103,** 365–378 (1999). doi: 10.1021/jp983150t

10. M.M. Maricq and J.J. Szente, "The $CH_3C(O)O_2$ radical. Its UV spectrum, self-reaction kinetics, and reaction with CH_3O_2", *J. Phys. Chem.* **100,** 4507–4513 (1996). doi: 10.1021/jp9533234

11. C.M. Roehl, D. Bauer and G.K. Moortgat, "Absorption spectrum and kinetics of the acetylperoxy radical", *J. Phys. Chem.* **100,** 4038–4047 (1996). doi: 10.1021/jp9526298

12. J. Sehested, L.K. Christensen, T. Mogelberg, O.J. Nielsen, T.J. Wallington, A. Guschin, J.J. Orlando and G.S. Tyndall, "Absolute and relative rate constants for the reactions $CH_3C(O)O_2$ + NO and $CH_3C(O)O_2$ + NO_2 and thermal stability of $CH_3C(O)O_2NO_2$", *J. Phys. Chem. A* **102,** 1779–89 (1998). doi: 10.1021/jp972881a

13. A. Tomas, E. Villenave and R. Lesclaux, "Reactions of the HO_2 radical with CH_3CHO and $CH_3C(O)O_2$ in the gas phase," *J. Phys. Chem. A* **105,** 3505–3514 (2001). doi: 10.1021/jp003762p

14. S.J. Zalyubovsky, B.G. Glover and T.A. Miller, "Cavity ringdown spectroscopy of the A–X electronic transition of the $CH_3C(O)O_2$ radical", *J. Phys. Chem. A* **107,** 7704–7712 (2003). doi: 10.1021/jp0305279

15. Y.J. Hu, H.B. Fu and E.R. Bernstein, "Generation and detection of the peroxyacetyl radical in the pyrolysis of peroxyacetyl nitrate in a supersonic expansion", *J. Phys. Chem. A* **110,** 2629–2633 (2006). doi: 10.1021/jp058196i

16. Y.J. Hu, H.B. Fu and E.R. Bernstein, "Vibronic spectroscopy of the peroxyacetyl radical in the near IR", *J. Chem. Phys.* **124,** 114305/1-05/6 (2006). doi: 10.1063/1.2179428

17. E.P. Clifford, P.G. Wenthold, R. Gareyev, W.C. Lineberger, C.H. DePuy, V.M. Bierbaum and G.B. Ellison, "Photoelectron spectroscopy, gas phase acidity, and thermochemistry of *tert*-butyl hydroperoxide: Mechanisms for the rearrangement of peroxyl radicals", *J. Chem. Phys.* **109,** 10293–10310 (1998). doi: 10.1063/1.477725

18. S.J. Blanksby, T.M. Ramond, G.E. Davico, M.R. Nimlos, S. Kato, V.M. Bierbaum, W.C. Lineberger, G.B. Ellison and M. Okumura, "Negative-ion photoelectron spectroscopy, gas-phase acidity, and thermochemistry of the peroxyl radicals CH_3OO and CH_3CH_2OO", *J. Am. Chem. Soc.* **123,** 9585–9596 (2001). doi: 10.1021/ja010942j

19. S.J. Blanksby, G.B. Ellison, V.M. Bierbaum and S. Kato, "Direct evidence for base-mediated decomposition of alkyl hydroperoxides (ROOH) in the gas phase", *J. Am. Chem. Soc.* **124,** 3196-97 (2002). doi: 10.1021/ja017658c

20. T.M. Ramond, S.J. Blanksby, S. Kato, V.M. Bierbaum, G.E. Davico, R.L. Schwartz, W.C. Lineberger and G.B. Ellison, "Heat of formation of the hydroperoxyl radical HOO via negative ion studies", *J. Phys. Chem. A* **106,** 9641–9647 (2002). doi: 10.1021/jp014614h

21. S.J. Blanksby, S. Kato, V.M. Bierbaum and G.B. Ellison, "Fragmentations of deprotonated alkyl hydroperoxides (ROO^-) upon collisional activation: a combined experimental and computational study", *Aust. J. Chem.* **56,** 459–472 (2003). doi: 10.1071/CH03039

22. S.J. Blanksby, V.M. Bierbaum, G.B. Ellison and S. Kato, "Superoxide does react with peroxides: direct observation of the Haber–Weiss reaction in the gas phase", *Angew. Chem.* **46,** 4948–4950 (2007). doi: 10.1002/anie.200700219

23. S. Kato, G.B. Ellison, V.M. Bierbaum and S.J. Blanksby, "Base-induced decomposition of alkyl hydroperoxides in the gas phase. Part 3. Kinetics and dynamics in the HO^- + CH_3OOH, C_2H_5OOH, and *tert*-C_4H_9OOH reactions", *J. Phys. Chem. A* **112,** 9516–9525 (2008). doi: 10.1021/jp800702z

24. S.M. Villano, N. Eyet, S.W. Wren, G.B. Ellison, V.M. Bierbaum and W.C. Lineberger, "Photoelectron spectroscopy and thermochemistry of the peroxyformate anion", *J. Phys. Chem. A,* in press (2009). doi: 10.1021/jp907569w

25. J. Berkowitz, G.B. Ellison and D. Gutman, "Three methods of measuring bond energies", *J. Phys. Chem.* **98,** 2744–2765 (1994). doi: 10.1021/j100062a009

26. S.J. Blanksby and G.B. Ellison, "Bond dissociation energies of organic molecules," *Acc. Chem. Res.* **36,** 255–263 (2003). doi: 10.1021/ar020230d

27. K.M. Ervin, S. Gronert, S.E. Barlow, M.K. Gilles, A.G. Harrison, V.M. Bierbaum, C.H. DePuy, W.C. Lineberger and G.B. Ellison, "Bond strengths of ethylene and acetylene", *J. Am. Chem. Soc.* **112,** 5750 (1990). doi: 10.1021/ja00171a013

28. P.G. Wenthold and W.C. Lineberger, "Negative ion photoelectron spectroscopy studies of organic reactive intermediates", *Acc. Chem. Res.* **32,** 597–604 (1999). doi: 10.1021/ar960121x

29. K.M. Ervin and W.C. Lineberger, "Photoelectron spectroscopy of negative ions", in *Advances in Gas*

Phase Ion Chemistry, Vol. 1, Ed by N.G. Adams and L.M. Babcock. JAI Press, Greenwich, Connecticut, USA, p. 121–166 (1992).

30. T.M. Ramond, G.E. Davico, R.L. Schwartz and W.C. Lineberger, "Vibronic structure of alkoxy radicals via photoelectron spectroscopy", *J. Chem. Phys.* **112,** 1158–1169 (2000). doi: 10.1063/1.480767

31. H. Hotop and W.C. Lineberger, "Binding energies in atomic negative-ions .2", *J. Phys. Chem. Ref. Data* **14,** 731–750 (1985).

32. J. Cooper and R.N. Zare, "Angular distribution of photoelectrons", *J. Chem. Phys.* **48,** 942–943 (1968). doi: 10.1063/1.1668742

33. J.M. Van Doren, S.E. Barlow, C.H. DePuy and V.M. Bierbaum, "The tandem flowing afterglow-sift-drift", *Int. J. Mass Spectrom. Ion Processes* **81,** 85–100 (1987). doi: 10.1016/0168-1176(87)80007-1

34. K.M. Ervin, "Experimental techniques in gas-phase ion thermochemistry", *Chem. Rev.* **101,** 391–444 (2001). doi: 10.1021/cr990081l

35. M.J. Frisch, G.W. Trucks, H.B. Schlegel, G.E. Scuseria, M.A. Robb, J.R. Cheeseman, J.A. Montgomery, T. Vreven, K.N. Kudin, J.C. Burant, J.M. Millam, S.S. Iyengar, J. Tomasi, V. Barone, B. Mennucci, M. Cossi, G. Scalmani, N. Rega, G.A. Petersson, H. Nakatsuji, M. Hada, M. Ehara, K. Toyota, R. Fukuda, J. Hasegawa, M. Ishida, T. Nakajima, Y. Honda, O. Kitao, H. Nakai, *Gaussian 03*. Gaussian Corporation, Pittsburgh, PA, USA (2003).

36. A.D. Becke, "Density functional thermochemistry. III. The role of exact exchange", *J. Chem. Phys.* **98,** 5648–5652 (1993). doi: 10.1063/1.464913

37. R. Krishnan, J.S. Binkley, R. Seeger and J.A. Pople, "Self-consistent molecular–orbital methods. XX. Basis set for correlated wave-functions", *J. Chem. Phys.* **72,** 650–654 (1980). doi: 10.1063/1.438955

38. C.T. Lee, W.T. Yang and R.G. Parr, "Development of the Colle–Salvetti Correlation-Energy Formula into a functional of the electron-density", *Phys. Rev. B* **37,** 785–789 (1988). doi: 10.1103/PhysRevB.37.785

39. A.G. Baboul, L.A. Curtiss, P.C. Redfern and K. Raghavachari, "Gaussian-3 theory using density functional geometries and zero-point energies", *J. Chem. Phys.* **110,** 7650–7657 (1999). doi: 10.1063/1.478676

40. K.M. Ervin, *Pescal*. University of Nevada, Reno, USA, (2003).

41. J.J. Grabowski and X.H. Cheng, "Gas-phase formation of the enolate monoanion of acetic-acid by proton abstraction", *J. Am. Chem. Soc.* **111,** 3106–3108 (1989). doi: 10.1021/ja00190a078

42. K.M. Ervin and V.F. DeTuri, "Anchoring the gas-phase acidity scale", *J. Phys. Chem. A* **106,** 9947–9956 (2002). doi: 10.1021/jp020594n

43. N. Eyet, S.M. Villano and V.M. Bierbaum, "Anchoring the gas-phase acidity scale: From formic acid to methanethiol", *Int. J. Mass Spectrom* **283,** 26–29 (2009). doi: 10.1016/j.ijms.2009.01.001

44. J.A. Cugley, W. Bossert, A. Bauder and H.H. Gunthard, "Microwave-spectrum, dipole-moment and barrier to internal-rotation of peroxyacetic acid", *Chem. Phys.* **16,** 229–235 (1976). doi: 10.1016/0301-0104(76)80058-4

45. C.H. DePuy, "Understanding organic gas-phase anion molecule reactions", *J. Org. Chem.* **67,** 2393–2401 (2002). doi: 10.1021/jo0163593

46. (a) J.D. Cox, D.D. Wagman, V.A. Medvedev, "$\Delta_f H_{298}(H_2O) = -242.40 \pm 0.04$ kJ mol^{-1}", *CODATA key values for thermodynamics*. Hemisphere Publishing Corporation, New York, USA, p. 1 (1984); (b) L.V. Gurvich; I.V. Veyts; C.B. Alcock; V.S. Iorish", $\Delta_f H_{298}(H_2O_2) = -136.2 \pm 0.2$ kJ mol^{-1}", in *Thermodynamic Properties of Individual Substances*, Vol. 1, 4th Edn. Hemisphere, New York, USA (1989); (c) S.J. Blanksby and G.M. Ellison, Reference 26, "$\Delta_f H_{298}(HOO) = 13.4 \pm 2.1$ kJ mol^{-1}"; (d) P.J. Linstrom and W.E. Mallard, "$\Delta_f H_{298}(CH_3CO_2H) = -433 \pm 3$ kJ mol^{-1}", in *NIST Chemistry WebBook*, *NIST Standard Reference Database* Number 69 Edn; National Institute of Standards and Technology: Gaithersburg, MD, USA 20899, (2005); (e) Z. Lu, "$\Delta_f H_{298}(CH_3CO_2) = \leqslant -175 \pm 4$ kJ mol^{-1}", Evaluated from a negative ion cycle: $EA(CH_3CO_2) \leqslant 3.47 \pm 0.01$ eV; R.E. Continetti, "Dynamics of the acetyloxyl radical studied by dissociative photodetachment of the acetate anion", *J. Phys. Chem. A* **108,** 9962–9969 (2004), N. Eyet, S.M. Villano and V.M. Bierbaum, Reference 43, "$\Delta_a H_{298}(CH_3CO_2H) = 1454 \pm 2$ kJ mol^{-1}" and P.J. Linstrom and W.E. Mallard (and see above) "$\Delta_f H_{298}(CH_3CO_2H) = -433 \pm 3$ kJ mol^{-1}"; (f) S.J. Blanksby and G.M. Ellison, Reference 26, "$\Delta_f H_{298}(CH_3) = 146.6 \pm 0.03$ kJ mol^{-1}"; (g) M.W. Chase, C.A. Davies, J.R. Downey, D.J. Frurip, R.A. McDonald and A.N. Syverud, "$\Delta_f H_{298}(CO_2) = -393.53 \pm 0.05$ kJ mol^{-1}", *JANAF Thermochemical Tables* 3rd Edn", *J. Phys. Chem. Ref. Data* **14,** (1985); (h) M.W. Chase, C.A. Davies, J.R. Downey, D.J. Frurip, R.A. McDonald and A.N. Syverud (see above), "$\Delta_f H_{298}(CO) = -110.53 \pm 0.17$ kJ mol^{-1}"; (i) S.J. Blanksby and G.M. Ellison, Reference 26, "$\Delta_f H_{298}(NO2) = 34.2 \pm 0.05$ kJ mol^{-1}"; (j) S.J. Blanksby and G.M. Ellison, Reference 26, "$\Delta_f H_{298}(NO_3) = -393.53 \pm 0.05$ kJ mol^{-1}"; (k) J. Berkowitz, G.B. Ellison and D. Gutman, Reference 25,"$\Delta_f H_{298}(CH_2CO) = -47.5 \pm 16$ kJ mol^{-1}"; (l) S.J. Blanksby and G.M. Ellison, Reference 26, "$\Delta_f H_{298}[HC(O)] = 42.2 \pm 0.5$ kJ mol^{-1}"; (m) S.J. Blanksby and G.M. Ellison, Reference 26, "$\Delta_f H_{298}[CH_3C(O)] = -10.0 \pm 1.3$ kJ mol^{-1}".

47. J.W. Bozzelli, C. Sheng, C.J. Chen and A.M. Dean, "Thermochemistry and kinetics for alkyl + O_2 reactions in hydrocarbon oxidation", *Abstr. Pap. Am. Chem. Soc.* **223,** U571–U772 (2002).

48. R. Benassi and E. Taddei, "Homolytic bond dissociation in peroxides, peroxyacids, peroxyesters

and related radicals—*ab initio* MO calculations", *Tetrahedron* **50,** 4795–4810 (1994). doi: 10.1016/S0040-4020(01)85017-1

49. *NIST Chemistry WebBook, NIST Standard Reference Database*, Vol. 69, edited by P.J. Linstrom and W.G. Mallard. National Institute of Standards and Technology, Gaithersburg, MD, USA, 20899 (2005).

50. G.S. Tyndall, R.A. Cox, C. Granier, R. Lesclaux, G.K. Moortgat, M.J. Pilling, A.R. Ravishankara and T.J. Wallington, "Atmospheric chemistry of small organic peroxyl radicals", *J. Geophys. Res., Atmos.* **106,** 12157–12182 (2001).

51. I.W.M. Smith and A.R. Ravishankara, "Role of hydrogen-bonded intermediates in the bimolecular reactions of the hydroxyl radical," *J. Phys. Chem. A* **106,** 4798–4807 (2002). doi: 10.1021/jp014234w

52. P.W. Bruckmann and H. Willner, "Infrared spectroscopic study of peroxyacetyl nitrate (PAN) and its decomposition products," *Environ. Sci. Technol.* **17,** 352–357 (1983). doi: 10.1021/es00112a009

53. C.E. Miller, J.I. Lynton, D.M. Keevil and J.S. Francisco, "Dissociation pathways of peroxyacetyl nitrate (PAN)," *J. Phys. Chem. A* **103,** 11451–11459 (1999). doi: 10.1021/jp992667h

54. I. Bridier, F. Caralp, H. Loirat, R. Lesclaux, B. Veyret, K.H. Becker, A. Reimer and F. Zabel, "Kinetic and theoretical studies of the reactions $CH_3C(O)O_2+NO_2+M \rightarrow CH_3C(O)O_2NO_2+M$ between 248 K and 393 K and between 30 Torr and 760 Torr," *J. Phys. Chem.* **95,** 3594–3600 (1991). doi: 10.1021/j100162a031